

# Chromophore dependence of intramolecular vibrational relaxation: Si–H stretch second overtone versus C–H stretch first overtone in methylsilane

J. W. Dolce, A. Callegari, B. Meyer,<sup>a)</sup> K. K. Lehmann, and G. Scoles  
*Department of Chemistry, Princeton University, Princeton, New Jersey 08544-1009*

(Received 2 December 1996; accepted 23 July 1997)

The intramolecular vibrational relaxation (IVR) of an excited Si–H stretch (second overtone) and C–H stretch (first overtone) in methylsilane has been examined by eigenstate resolved infrared spectroscopy. The experiment probes a molecular beam produced in a supersonic expansion, excited by a laser in a power buildup cavity, and detected by a liquid helium cooled silicon bolometer. The Si–H stretch [local mode (3,0,0), both *A* and *E* combinations] is compared with the nearly isoenergetic C–H stretch [predominantly the  $2\nu_7^0$  band]. With the calculated density of states almost unchanged, the two modes exhibit very different IVR behavior, which is quantified in terms of the lifetime of the bright states and the coupling between the bright states and the dark states. © 1997 American Institute of Physics. [S0021-9606(97)00541-2]

## I. INTRODUCTION

The study of intramolecular vibrational relaxation (IVR) is of fundamental importance to our understanding of chemical reactions at the molecular level. Although simple statistical models<sup>1</sup> have been very successful in explaining the reaction rates of a large class of unimolecular reactions, their range of applicability is still not precisely defined. In order to understand in greater detail the dynamics of a wider variety of reactions, and accurately assess the possibility of controlling chemical reactions, IVR in isolated molecules continues to be the object of intensive investigations. The field has been reviewed recently by Lehmann *et al.*<sup>2</sup> and by Nesbitt and Field.<sup>3</sup> The most frequently used experimental method is that of eigenstate-resolved spectroscopy in which the spectral fragmentation of the optically active state caused by the mixing with the “dark” bath states is measured using high-resolution spectroscopy. The time-dependent picture of the energy localization out of the optically active state is then obtained by Fourier transformation of the spectrum autocorrelation.<sup>4</sup>

In order to facilitate comparison between theory and experiment, it is natural to compare the decay rates of different nearly isoenergetic vibrational states within the same molecule. In this way, the bath states are a constant in the comparison, and differences in behavior can be attributed to the nature and strength of the couplings of the bright state to the bath. A few molecules have been studied from this perspective, e.g., diacetylene,<sup>5</sup> propyne<sup>6–8</sup> 1-butyne,<sup>9,10</sup> and 1-pentyne.<sup>9</sup> In diacetylene, the  $\nu = 3$  spectra of the acetylenic stretches [(2,1)<sup>+</sup> and (3,0)<sup>+</sup>] have been measured. The lifetime of (2,1)<sup>+</sup> ranges from 0.39 to 6.58 ns, depending on the upper state angular momentum. The lifetime of (3,0)<sup>+</sup> ranges from 70 to 215 ps. The pure overtone has a significantly shorter lifetime than the delocalized combination

band. A similar effect has been observed in propyne<sup>7</sup> where  $3\nu_1$  is significantly more perturbed than  $\nu_1 + 2\nu_6$  and<sup>11</sup>  $2\nu_1 + \nu_6$  (Here  $\nu_1$  is the acetylenic hydrogen stretch and  $\nu_6$  the asymmetric methyl stretch). In both molecules, the phenomenon is believed to be related to the fact that the combination modes are basically composed of two dynamically independent chromophores, since the modes in the delocalized state do not move common atoms. Thus, the chromophores are only weakly anharmonically coupled and relax independently. Since the components of the combination mode are more harmonic than the localized state, the combination mode relaxes more slowly. This behavior can be contrasted with the phenomenon of enhanced stability of extreme motion states in which vibrational overtones of a chromophore have been found (as predicted) to decay less rapidly than isoenergetic combination bands when all atoms involved belong to the same group.<sup>12–14</sup>

In the particular case where the vibrational excitation is localized in a specific chromophore, comparison between different chromophores in the same molecule gives information about whether or not the dynamics are mode specific. One example of this is 1-butyne, in which the  $\nu = 1$  spectra of the acetylenic hydrogen stretching mode and the asymmetric methyl stretching mode have been measured. The modes have lifetimes of 269 and 276 ps, respectively, indicating very similar IVR. The same kind of comparison in 1-pentyne gives a lifetime for the methyl stretch 5–10 times shorter than the 440 and 760 ps for the acetylenic stretch (respectively of the gauche and trans conformer). In a similar way the  $\nu = 2$  spectra of the acetylenic hydrogen stretch and the methyl stretch of propyne can be compared. The modes have lifetimes of 200<sup>15</sup> and 31 ps,<sup>6</sup> respectively, indicating significantly different IVR. The reasons for these results can be speculated upon. It has been proposed by both McIlroy<sup>16</sup> and by Bethardy and Perry<sup>10</sup> that the differences between 1-butyne and 1-pentyne are a consequence of the presence in the latter of a low energy isomerization pathway. This argument cannot be used to rationalize the observed enhanced

<sup>a)</sup>On leave from the University of Bonn, Institut für Angewandte Physik, Wegelerstr. 8, 53115 Bonn, Germany.

TABLE I. The tier structure enumerated for methylsilane. Column  $V$  lists the total number of quanta in a state, and represents the tier order; a) energy range of  $5860\text{--}5960\text{ cm}^{-1}$ , corresponding to  $2\nu_7^0$ ; b) energy range of  $6250\text{--}6350\text{ cm}^{-1}$ , corresponding to  $(3,0,0)$ .

a			
$V$	A1	A2	$E$
2	0	0	1
3	0	0	0
4	17	16	31
5	92	91	196
6	168	169	329
7	259	257	516
b			
$V$	A1	A2	$E$
2	0	0	0
3	0	0	0
4	20	16	38
5	107	104	206
6	181	179	363
7	347	347	705

IVR of the methyl group relative to that of the acetylenic hydrogen stretch in the case of propyne. One possible explanation for this result is the presence of a stretch–bend Fermi resonance<sup>17,18</sup> in the methyl group that is, two quanta of methyl deformation may provide a quasi-resonant “doorway” state to the bath for one quantum of stretch.

The experiment reported here compares the high-resolution infrared spectrum of two motions in methylsilane: The  $2\nu_7^0$  [asymmetric methyl stretch] and the  $(3,0,0)$  [three quanta in one Si–H bond]. Since the motions are nearly isoenergetic, the total density of states is comparable. In fact, the densities of lower order resonances are similar too (see Table I). Thus, differences in behavior can be attributed to the nature of the couplings and their strength.

The two vibrations being considered here are actually quite different, as indicated by the different notations. The Si–H stretch at  $\nu=3$  is very much a local oscillator, whereas the C–H stretch at  $\nu=2$  is closer to a normal mode than to a local mode. The evidence for the local mode character of Si–H stretches comes from the rovibrational spectrum of molecules containing this bond, such as silanes and methyl substituted silanes. In silane, more than two quanta in Si–H stretches break the symmetry of the spherical top, giving rise to a symmetric top spectrum.<sup>19</sup> This is compelling evidence for describing the motion as  $(\nu,0,0,0)$ . In methylsilane, a similar local mode behavior occurs. The spectrum of methylsilane in the  $\nu=3$  Si–H overtone region shows just one band, assigned as  $(3,0,0)$ .<sup>20</sup> Furthermore, the splitting of the fundamental frequencies of the symmetric and asymmetric Si–H stretches<sup>21</sup> is only  $4\text{ cm}^{-1}$ . On the other hand, the C–H motion at  $\nu=2$  in methylsilane has a large normal mode component.<sup>22</sup> Clearly, the Si–H and C–H stretches have rather different character, which could profoundly influence their coupling to the bath and, therefore, their IVR rates.

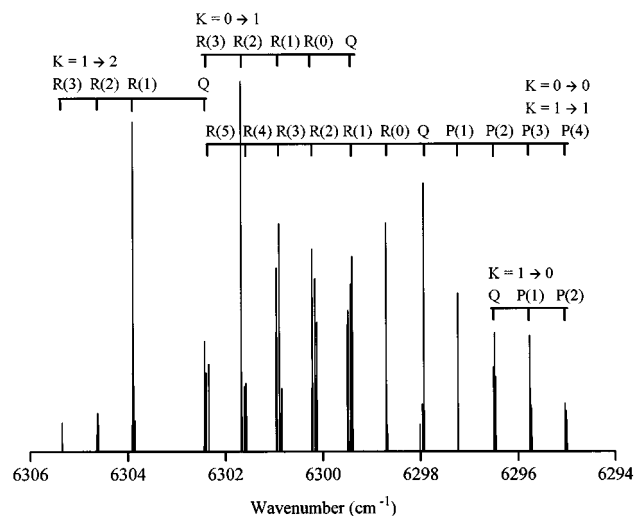


FIG. 1. A stick spectrum of the  $(3,0,0)$  band of methylsilane Si–H stretch second overtone.

## II. EXPERIMENT

The high-resolution infrared spectra were obtained using a molecular beam spectrometer with optothermal detection which has been described in a previous paper.<sup>23</sup> Briefly, a beam of the molecule of interest is excited with a tunable infrared laser and the excitation is detected downstream by means of a cryogenically cooled bolometer. The beam is formed by expanding a 1% mixture of methylsilane<sup>24</sup> in helium at a stagnation pressure of 0.48 MPa through a  $50\text{ }\mu\text{m}$  diam nozzle. The laser is a stabilized  $1.5\text{ }\mu\text{m}$  color center laser, tuned in 1 MHz increments at a rate of about 20 MHz/s. The laser frequency is monitored with a wave meter and two scanning etalons of 8 GHz and 150 MHz free spectral range (FSR), respectively. The 150 MHz etalon is temperature stabilized and serves as a frequency reference.

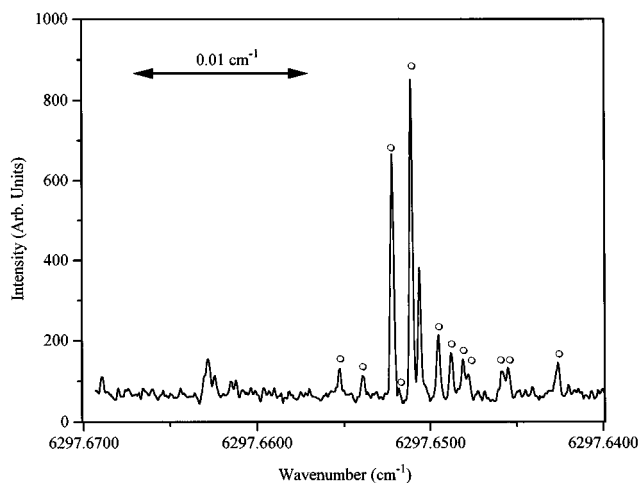


FIG. 2. A magnified view of the  ${}^qQ_1$  branch of the  $(3,0,0)$  band of methylsilane Si–H stretch second overtone. The  $J''=1$  portion is highlighted by circles.

TABLE II. The results of rigid rotor fits to the subbands of (3,0,0).

Subband	Origin (cm <sup>-1</sup> )	$\Delta B$ (cm <sup>-1</sup> )	Stand. dev. (MHz)	Number of points
$K=0 \rightarrow 0$	6297.6908 (4)	$6.2 \times 10^{-4}$ (2)	24	10
$K=1 \rightarrow 1$	6297.6542 (8)	$-8.0 \times 10^{-4}$ (5)	37	7
$K=0 \rightarrow 1$	6299.2038 (35)	$-9.0 \times 10^{-4}$ (3)	119	4
$K=1 \rightarrow 2$	6302.1507 (79)	$-5.3 \times 10^{-4}$ (6)	17	3

The laser excitation occurs inside a resonant power buildup cavity<sup>25</sup> located across the molecular beam. Construction details have been reported previously.<sup>5</sup> The laser is coupled to the cavity through a single mode fiber. Effective mode matching is achieved via a GRIN lens located between the cavity and the fiber output. The effective power enhancement is about 600. The instrumental linewidth (about 6 MHz) is determined primarily by transit time broadening and residual Doppler broadening which are estimated to be 2.6 and 2.7 MHz, respectively.<sup>5</sup> Use of the buildup cavity made possible the observation of the weak (3,0,0) band with a signal-to-noise ratio of about ten. This band is about 20 times weaker than the  $2\nu_7^0$  band as estimated from integrated band strengths of an Fourier-transform infrared spectrum. [The  $2\nu_7^0$  band was not observed with a signal-to-noise ratio of 200, however, because the buildup cavity's finesse, and thus power buildup factor, in this region is eight times lower than in the (3,0,0) region.]

The spectrum of the (3,0,0) band was calibrated both in relative and absolute terms. The relative calibration was accomplished with the 150 MHz scanning etalon. The actual value of the etalon FRS was determined as the one which minimized the errors in the ground-state combination differences of the parallel subband, using a value for  $B'' = 10\,986.0853(52)$  MHz from microwave and far-IR spectroscopy.<sup>26</sup> Results of the combination difference fits are presented in the next section. The absolute calibration was accomplished with the wave meter, using the  $^7R_0(2)$  line at

6301.397 29 cm<sup>-1</sup> as reference point. The wave meter was calibrated with the  $P(1)$  line of acetylene, at 6554.111 767 cm<sup>-1</sup>. The wave meter readings were precise to  $\pm 0.0005$  cm<sup>-1</sup>.

For the spectrum of the  $2\nu_7$  band, the 150 MHz etalon was left uncalibrated. However, the whole spectrum was shifted with an additive factor in order to make the wave number scale at the  $R(0)$  branch (5908.006 23 cm<sup>-1</sup>) read accurately. In this way, the inaccuracy of the wave number scale across the whole spectrum is minimized.

### III. RESULTS

#### A. The spectra

The (3,0,0) band is shown in Fig. 1. Its assignment was completed by ground-state combination differences. Both parallel and perpendicular subbands are present. Lines and assignments are listed in Appendix A. A magnified picture of the  $^qQ_1$  branch is shown in Fig. 2. The spectrum shows sparse to intermediate fragmentation due to IVR. Each bright state is observed to be coupled to up to 15 dark states. In all cases, the lines are well resolved. Generally, the degree of fragmentation appears to increase with  $K'$ .

The quality of the data was assessed by fitting ground-state combination differences in the parallel subband. The following parameters were used:  $B''$  as given above, and  $D''_{JK} = 45.628$  kHz.<sup>26</sup> The fit has a standard deviation of 31 MHz. The quality of the assignment was assessed by fitting the spectrum to a rigid rotor model. The location of each bright state was taken as the centroid of its IVR multiplet. The following parameters were used:  $B''$  as given above,  $D''_J = 10.9114$  kHz,<sup>26</sup>  $D''_{JK}$  as given above,  $D'_J = D''_J$ , and  $D'_{JK} = D''_{JK}$ . The results of independent fits to each component of the parallel subband are presented in Table II. The standard deviation is 24 MHz for the  $K=0$  component and 37 MHz for the  $K=1$  component. These results are comparable to those obtained in the past with this spectrometer for other symmetric top molecules.<sup>27,28</sup> Independent fits to two

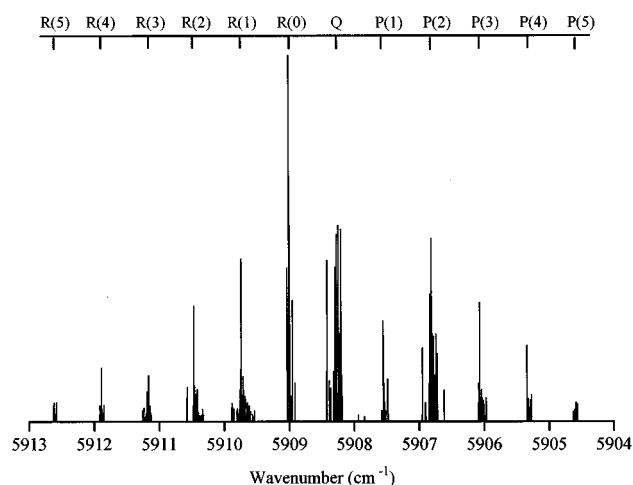


FIG. 3. A stick spectrum of the  $2\nu_7^0$  band of methylsilane C-H stretch first overtone.

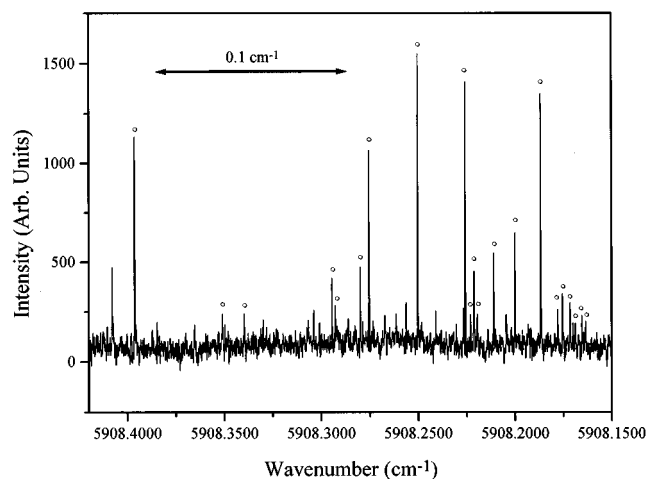


FIG. 4. A magnified view of the  $^qQ_1$  branch of the  $2\nu_7^0$  band of methylsilane C-H stretch first overtone. The  $J'' = 1$  portion is highlighted by circles.

TABLE III. A summary of the results of a Lawrence–Knight deconvolution, showing the extent and strength of the couplings between the various bright states and the observed  $N_d$  bath states. a) Silyl Group, A vibrational species; b) Silyl group, E vibrational species; c) Methyl group,  $2\nu_7$ .

a				
$K'$	$J'$	$N_d$	$\Delta E$ (cm $^{-1}$ )	$W_{\text{rms}}^2$ ( $10^{-3}$ cm $^{-1}$ )
0	6	1	...	0.90
	5	3	0.0052	1.6
	4	1	...	0.86
	3	1	...	0.58
	2	3	0.0050	0.92
	1	4	0.0075	1.4
	0	1	...	0.76
				1.0
1	5	4	0.011	3.1
	4	10	0.017	1.5
	3	3	0.0096	2.2
	2	6	0.010	1.1
	1	12	0.012	0.76
				1.76
b				
$K'$	$J'$	$N_d$	$\Delta E$ (cm $^{-1}$ )	$W_{\text{rms}}^2$ ( $10^{-3}$ cm $^{-1}$ )
0	0	4	0.0088	2.5
	1	2	0.0072	2.9
				2.7
1	4	1	...	1.4
	3	7	0.024	2.3
	2	6	0.0079	1.1
	1	5	0.018	2.5
				1.8
2	4	4	0.0013	0.27
	3	13	0.037	3.2
	2	15	0.053	3.0
				2.2
c				
$K'$	$J'$	$N_d$	$\Delta E$ (cm $^{-1}$ )	$W_{\text{rms}}^2$ ( $10^{-3}$ cm $^{-1}$ )
0	0	7	0.10	10
0	1	5	0.11	11
1	1	20	0.22	22

components of the perpendicular subband are also presented in Table II. The standard deviation is 119 MHz for the  $K=0 \rightarrow 1$  subband, and 17 MHz for the  $K=1 \rightarrow 2$ .

The  $2\nu_7^0$  band is shown in Fig. 3.  $J''$  was assigned to each clump by ground-state combination differences. All of the major lines belong to a parallel subband. Several very weak lines, which could not be assigned, indicate the probable presence of a weak perpendicular subband.  $K''$  could generally not be assigned; the difference between the upper and lower state rotational constants is insufficient to offset the extensive fragmentation of each  $P(J'')$  and  $R(J'')$  branch, resulting in  $K''$  clumps which are thoroughly intermingled. However, there are some special cases for which  $K''$  could be assigned. The  $R(0)$  and  $P(1)$  necessarily belong to  $K''=0$ . The  $Q$  branch belongs to  $K''=1$  only, because the  $(3,0,0)$  spectrum shows that only  $K''=0$  and 1 are populated. For  $P(2)$ , the  $K''=0$  and 1 components could be distinguished, because the  $K''=1$  lines appear in the  $Q$  branch. In a further effort to assign  $K''$ , the intensity ratios of the  $P$  and  $R$  branches were computed. Some evidence of a

bimodal distribution ( $K''=0,1$ ) is present but the distinction between the two groups is insufficient for a definite assignment. Consequently, quantum numbers could only be assigned for three upper states:  $(J',K')=(0,0)$ ,  $(1,0)$ , and  $(1,1)$ . The assignments are listed in Appendix B.

These three clumps will be treated as being representative of the whole spectrum of the methyl group. The IVR present in  $2\nu_7^0$  is clearly more extensive than that in  $(3,0,0)$ . For illustration, the  ${}^4Q_1$  branch is shown in Fig. 4 and should be compared with that of  $(3,0,0)$  in Fig. 2. This comparison of the  $Q$  branches for the two modes shows that the number of coupled dark states is 20 versus 12. Also, the breadths of the  $Q$  branches differ by a factor of about 20. Comparisons made for the other states yield similar results.

## B. Coupling strengths

In order to determine the strengths of the couplings between the bright states and the dark states, a Lawrence–Knight deconvolution,<sup>29,30</sup> has been performed. Technically, the procedure can only be used if unique quantum numbers can be assigned to each line. Here, the torsional quantum numbers are not assigned. However, if the zero-order torsional splitting is small, neglecting this detail should only result in a slight overestimate of the clump width. The results for both modes are summarized in Table III. For  $(3,0,0)$  the matrix elements range from  $0.6 \times 10^{-3}$  cm $^{-1}$  to  $3.2 \times 10^{-3}$  cm $^{-1}$ . For  $2\nu_7^0$ , the couplings range from  $10 \times 10^{-3}$  cm $^{-1}$  to  $20 \times 10^{-3}$  cm $^{-1}$ , roughly ten times as large.

Three possible coupling mechanisms are considered here: Anharmonic ( $W_a$ ), parallel ( $W_{\parallel}$ ), and perpendicular ( $W_{\perp}$ ) Coriolis coupling. The rotational dependence of the coupling coefficients can be examined in order to infer the nature of the coupling mechanism(s) since  $W_a$  is independent of  $J', K'$ , while  $W_{\parallel}$  is linear in  $K'$  and  $W_{\perp}$  is proportional to  $\sqrt{(J'-K')(J'+K'+1)+(J'+K')(J'-K'+1)}$ . For  $(3,0,0)$ , there are enough data so that the statistics are signifi-

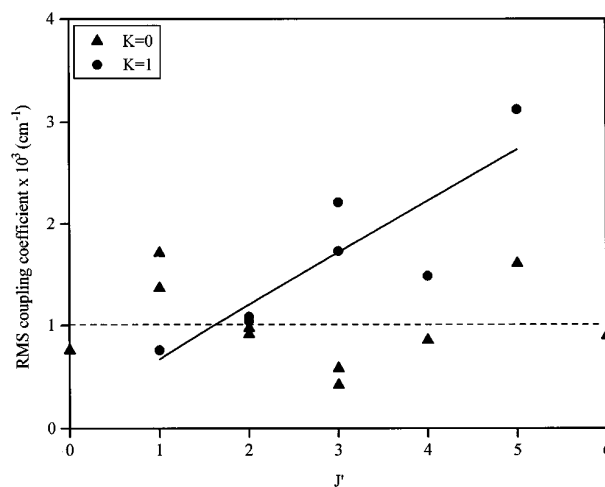


FIG. 5. The  $J'$  dependence of the rms coupling energy for the  $(3,0,0)$  parallel subband of methylsilane Si–H stretch second overtone. The best fit functions (see text for details) are also plotted.

cant. In the case of the parallel band, the results are plotted in Fig. 5. The  $K=0$  component shows no systematic  $J'$  dependence, indicating an anharmonic coupling mechanism. Fitting a constant function to the data gives  $W_a = 1.0 \pm 0.13$

$\times 10^{-3} \text{ cm}^{-1}$ . The  $K=1$  component exhibits an approximately linear  $J'$  dependence, suggesting an additional contribution from perpendicular Coriolis coupling. Assuming this to be the case, the r.m.s. coupling  $W$  would be

$$\sqrt{\frac{\rho_{K=1}(W_a^2 + W_{\parallel}^2) + \rho_{K=2}W_{\perp}^2[J(J+1)] + \rho_{K=0}W_{\perp}^2[J(J+1)-2]}{\rho_{K=1} + \rho_{K=2} + \rho_{K=0}}} \quad (1)$$

A fit of this function to the data gives  $(W_a^2 + W_{\parallel}^2)^{1/2} = 0.76 \pm 1.0 \times 10^{-3} \text{ cm}^{-1}$  and  $W_{\perp} = 0.6 \pm 0.07 \times 10^{-3} \text{ cm}^{-1}$ , which indicates that perpendicular Coriolis coupling dominates for  $J \geq 1$ . Because of the small number of  $K$  subbands observed the data does not give much insight about parallel Coriolis coupling since its contribution (if any) for  $K'=1$  is smaller than the error of the fit.

### C. Density of states

Information on the coupling between the bright state and the bath can also be obtained by comparing the available density of states with the observed coupled density of states. The available vibrational density of states was calculated from a harmonic oscillator model, using a numerical inverse Laplace transform method.<sup>31</sup> The fundamental frequencies<sup>32,33</sup> are listed in Table IV. The torsional coordinate was treated as a vibrational mode with threefold symmetry. Although a harmonic oscillator model underestimates the true density of states, usually the discrepancy becomes significant only at high vibrational energies. For example in trifluoropropyne at  $\nu_{\text{CH}} = 1,2$  the harmonic model has been estimated<sup>28</sup> to account for  $\sim 90\%$  of the anharmonic vibrational density of states. The actual coupled density of states  $\rho$  can be calculated from the spectrum in various ways. The simplest and most direct measure is

$$\rho = (N-1)/\Delta E, \quad (2)$$

where  $N$  is the number of eigenstates, and  $\Delta E$  is the energy window in which the ‘‘multiplet’’ appears.<sup>15</sup> For real spectra this measure is a little bit crude, because the limited signal-to-noise ratio leads to an underestimate of  $N$ . Another measure, which accounts for the finite signal to noise ratio, is

$$\rho = \frac{\sum(1/W_i)}{2\sqrt{S/N}}, \quad (3)$$

where  $W_i$  is the average coupling strength, and  $S/N$  is the signal to noise ratio.<sup>15</sup> The signal  $S$  is taken as the intensity of the strongest line, and the noise  $N$  is taken as the intensity of the weakest line which would be accepted as a line. Equation (3) is valid for the ‘‘sparse’’ regime, in which  $W_{\text{rms}} \cdot \rho < 1/2$ . While the  $2\nu_7^0$  mode is generally outside of this domain, the (3,0,0) mode satisfies this criterion. However, since the coupling coefficients are so small, the computed density turns out to be unphysically large. For this reason, the coupled density of states is calculated by Eq. (2), keeping in

mind that the result is an underestimate of the true value. The coupled densities of states are compared with the estimated densities of states in Tables V and VI. The results for each mode are considered in turn.

The  $2\nu_7^0$  mode shows coupled densities of states which are significantly less than the estimated density of  $A$  symmetry vibrational states: Only 36%–71%. This suggests that the bright state is only coupled to a subset of the states allowed by symmetry. The (3,0,0) mode shows a more complicated behavior. The coupled densities of states are often larger than expected and exhibit large variations with  $J'$ . To simplify the analysis, averages over  $J'$  are considered first. For the  $A$  vibrational species, the average coupled density of states is about 90% of the total available density of vibrational states. This indicates an extensive coupling between  $A$  and  $E$  symmetries, and is consistent with a perpendicular type Coriolis interaction. For the  $E$  vibrational species, the  $K'=0$  and 1 levels have an average coupled density of states which approaches or slightly exceeds the  $E$  component of the available density of states, suggesting that the coupling is only to dark states of  $E$  symmetry. For  $K'=2$  the average coupled density of states exceeds the total available vibrational density by about 70%. This could be due to a coupling to the  $(2J+1)K$  states by Coriolis coupling mechanism. With this factor of  $(2J+1)$  to account for the full density of rovibrational states of appropriate symmetry, the coupled density of states is within the expected range. Although not so common in rigid molecules, the phenomenon of extensive  $K$  mixing

TABLE IV. The normal modes and fundamental transitions of methylsilane.

Symmetry	Mode	Description	Wave number ( $\text{cm}^{-1}$ )
$A_1$	$\nu_1$	$\text{CH}_3$ stretch	2926.90
	$\nu_2$	$\text{SiH}_3$ stretch	2169.75
	$\nu_3$	$\text{CH}_3$ deformation	1263.56
	$\nu_4$	$\text{SiH}_3$ deformation	943.16
	$\nu_5$	$\text{SiC}$ stretch	702.99
$A_2$	$\nu_6$	torsion	190
$E$	$\nu_7$	$\text{CH}_3$ stretch	2981.67
	$\nu_8$	$\text{SiH}_3$ stretch	2165.78
	$\nu_9$	$\text{CH}_3$ deformation	1432.62
	$\nu_{10}$	$\text{SiH}_3$ deformation	952.5
	$\nu_{11}$	$\text{CH}_3$ rock	872.13
	$\nu_{12}$	$\text{SiH}_3$ rock	524.00

TABLE V. A comparison of the observed coupled density of states  $\rho_{\text{obs}}$  with the expected available density of states for  $2\nu_7^0$ . The column  $\rho_{90\%}$  gives the 90% confidence interval for  $\rho_{\text{obs}}$  based on the assumption that the states are distributed in energy according to Poisson statistics.

Bright state			
$K'$	$J'$	$\rho_{\text{obs}}$ (states/cm <sup>-1</sup> )	$\rho_{90\%}$
0	0	69	34–113
0	1	43	19–75
1	1	86	58–119
Calculated density of states			
A Type			121
E Type			241
Total			362

has been observed before, (e.g., by McIlroy and Nesbitt<sup>34</sup> in 1-butene and in the propyne  $3\nu_1$  spectrum). Given the very weak anharmonic coupling of the Si–H mode, it is not surprising that even a relatively weak  $K$  mixing can be observed

TABLE VI. A comparison of the observed coupled density of states  $\rho_{\text{obs}}$  with the expected available density of states for (3,0,0). The column  $\rho_{90\%}$  gives the 90% confidence interval for  $\rho_{\text{obs}}$  based on the assumption that the states are distributed in energy according to Poisson statistics.

Bright state			
$K'$	$J'$	$\rho_{\text{obs}}$ (states/cm <sup>-1</sup> )	$\rho_{90\%}$
A type	0	6	374
		5	473
	average	4	389
		3	742
		2	535
		1	507
		0	638
		523	
E type	1	5	247
		4	544
	average	3	249
		2	535
		1	951
			505
		0	1
0	329		
	258		
1	4		292
	3		285
	2	717	
2	1	258	
		388	
	4	2350	
	3	323	
average	2	276	
		984	
Calculated density of states			
A Type			188
E Type			376
Total			564

TABLE VII. Lifetimes of the bright states.

Bright state	Silyl group (3,0,0)	Lifetime (ns)
$K'$		averaged over $J'$
0	A Type	2.0
	E Type	1.3
1		0.87
		0.85
		1.9
Methyl group $2\nu_7^0$		
$K'$	Bright state	Lifetime (ps)
0	0	190
0	1	150
1	1	82

in the spectrum. The erratic variations in the coupled density of states with  $J'$  and  $K'$  is possibly due to random fluctuations of the bath density, as can be seen from the 90% confidence interval in Table VI. The striking difference in the fraction of coupled states that the two modes exhibit is more puzzling, since they couple with bath states that are expected to share almost the same average properties. Several explanations are possible: The high degeneracy of the bath states for symmetric top molecules in the harmonic approximation can produce large local variations of the density of states as observed for allene.<sup>35</sup> Also local mode  $A-E$  rotational coupling<sup>36</sup> could break down the  $C_{3v}$  vibrational symmetry thereby allowing coupling to a higher density of bath states. Last, because of the finite signal to noise, very weakly coupled states would inevitably disappear into the noise. It is not possible to quantify exactly to which extent this is relevant to our case but of the two spectra the one which is most likely to be affected is the one for the C–H stretch, since the oscillator strength is distributed into IVR multiplets that are on average ten times wider.

#### D. Time evolution of the bright state

The lifetimes of the bright states were determined by simulating a short pulse experiment by Fourier transforming the spectrum autocorrelation function and fitting a single exponential function to the decay of the survival probability  $P(t)$  thus obtained. The functional form used was

$$P(t) = c + Ae^{-t/\tau}, \quad (4)$$

with the constraint that  $c + A = 1$ .

The  $1/e$  time constants,  $\tau$ , are tabulated in Table VII. For the (3,0,0) state, the curves were actually averaged over  $J'$  in order to damp the recurrences. The lifetimes, for the parallel subband, range from 1.3 to 2.0 ns, for the perpendicular subband, from 0.85 to 1.9 ns. In contrast, the  $2\nu_7^0$  state shows dramatically shorter lifetimes: 82–190 ps. If the decay curves for the  $K=1$  component of the parallel subband of (3,0,0) are examined without averaging over  $J'$ , evidence for

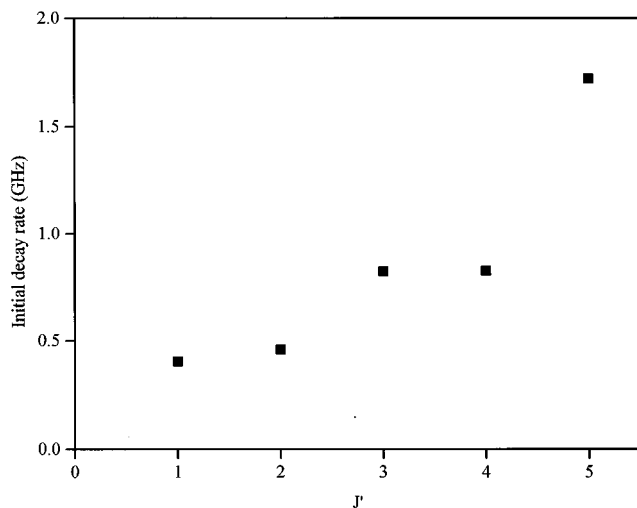


FIG. 6. The  $J'$  dependence of the initial decay rate for the  $K=1$  component of the (3,0,0) parallel subband of methylsilane.

Coriolis coupling should be evident, as claimed in the section on coupling strengths. The result is plotted in Fig. 6. The initial decay rates ( $\Gamma = 1/2\pi\tau$ ) clearly increase monotonically with  $J'$ .

#### IV. DISCUSSION

The results presented above consistently show that the IVR of the (3,0,0) and  $2\nu_7^0$  states are significantly different. The (3,0,0) state is coupled by anharmonic and Coriolis forces to a few to several dark states, over a range of  $0.01\text{ cm}^{-1}$ , with an average strength ( $W$ ) of  $\approx 1 \times 10^{-3}\text{ cm}^{-1}$ . The  $2\nu_7^0$  state is coupled to several to many dark states over a range of  $0.1\text{ cm}^{-1}$ , with an average strength of  $\approx 10 \times 10^{-3}\text{ cm}^{-1}$ , about ten times larger. Given the same density of coupled states ( $\rho$ ), from Fermi's Golden Rule

$$\Gamma = \frac{2\pi}{h} \langle W^2 \rangle \rho, \quad (5)$$

one would expect the decay rate for the C–H stretch to be about 100 times faster than for the Si–H stretch, in disagreement with the observed lifetimes. The discrepancy is removed if we consider that the actual density of coupled states is 6–9 times higher for (3,0,0) than it is for  $2\nu_7^0$  which partially compensates for the difference in coupling strengths.

The different behavior of these states is probably due to the way in which each mode couples to the bath, since the average properties of the bath are expected to be very similar in the two cases. One possibility is the presence of a strong, low-order anharmonic resonance, a doorway state,<sup>9</sup> for the methyl group, and the lack thereof for the silyl group. A prime candidate for a doorway state is the stretch–bend Fermi resonance, which is absent in the silyl group. Such

TABLE VIII. Lifetimes of nearly isoenergetic modes in a few molecules.

Molecule	Hydrogen group	Lifetime	Reference
CH <sub>3</sub> SiH <sub>3</sub>	Methyl, $\nu=2$	110 ps	This work
	Silyl, $\nu=3$	1.4 ns	This work
CH <sub>3</sub> CCH	Methyl, $\nu=2$	31 ps	2
	Acetylenic, $\nu=2$	200 ps	2
CH <sub>3</sub> CH <sub>2</sub> CCH	Methyl, $\nu=1$	276 ps	6
	Acetylenic, $\nu=1$	269 ps	6

resonances are known to be strong and nearly resonant for methylenic hydrogens.<sup>17,18</sup> For Si–H bonds, the resonance is poor: Two quanta of bending motion amounts to  $1892\text{ cm}^{-1}$  (neglecting anharmonicity), which is  $277\text{ cm}^{-1}$  lower than the stretching fundamental at  $2169\text{ cm}^{-1}$ . Thus, the coupling of  $3\nu_{\text{stretch}}$  to  $2\nu_{\text{stretch}} + 2\nu_{\text{bend}}$  is expected to be relatively weak. The weakness of the anharmonic coupling could account for another coupling mechanism becoming important, namely Coriolis coupling. The explicit  $J$  dependence of the coupling matrix elements, for  $K=1$ , indicates that the bright state couples to the bath directly by a Coriolis mechanism. Of course, an anharmonic contribution is probably present, too.

The presence of a Coriolis coupling mechanism has also been observed in other experiments, however, it is generally of minor importance for more rigid molecules and its dominance over the generally ubiquitous anharmonic mechanism for such an anharmonic motion and at such low  $J$  is unusual. However, a direct Coriolis coupling mechanism has been observed before, for example, in formaldehyde<sup>37</sup> and ethanol.<sup>38</sup> One possible explanation could be the lack of low-order resonances for coupling the Si–H stretch to other modes, which is consistent with the local mode character of the group.

These results for methylsilane can be compared with the results of other experiments in which different modes in the same molecule were examined. Such a comparison is made in Table VIII. It is interesting to note that in propyne, the acetylenic and methyl groups exhibit IVR which is analogous to that of the silyl and methyl groups in methylsilane, respectively. In addition, the analogy extends to the local and normal character of the modes, i.e., the silyl and acetylenic stretches have more local mode character than the methyl stretch, at these energies. However, in the case of 1-butyne  $\nu_{\text{CH}}=1$ , the analogy does not hold. Of course, 1-butyne has lower frequency skeletal motions than either methylsilane and propyne, so the nature of the bath states may not be comparable. It is tempting to generalize these results to all normal and local modes. That is, a local mode could be expected to be intrinsically more resistive to IVR. In methylsilane, since the harmonic or anharmonic couplings among the Si–H bonds are inherently weak, the anharmonic coupling to the rest of the molecule, via the silyl group, could be expected to encounter a “bottleneck.” In the acetylenes, the lone hydrogen is effectively isolated from the rest of the molecule, again requiring a high-order resonance in order to

TABLE IX. Lifetimes of methyl groups in a variety of molecules. The vibrational level is  $\nu = 1$ , unless otherwise indicated.

Molecule	Lifetime	Reference
CH <sub>3</sub> SiH <sub>3</sub> , $\nu = 2$	110 ps	This work
CH <sub>3</sub> CCH	n/a <sup>a</sup>	4
CH <sub>3</sub> CCH, $\nu = 2$	31 ps	2
CH <sub>3</sub> CH <sub>2</sub> CCH	276 ps	6
CH <sub>3</sub> CH <sub>2</sub> OH	59 ps	35
CH <sub>3</sub> CH <sub>2</sub> CHCH <sub>2</sub>	>31 ps	6
CH <sub>3</sub> CH <sub>2</sub> CH <sub>2</sub> CH <sub>3</sub>	>18 ps	6
CH <sub>3</sub> CH <sub>2</sub> CH <sub>3</sub>	265 ps	6
(CH <sub>3</sub> ) <sub>2</sub> CHCH <sub>3</sub>	>177 ps	6
CH <sub>3</sub> CHCHCH <sub>3</sub> (trans)	132 ps	6

<sup>a</sup>No fragmentation of the spectrum was observed.

couple to the bath. In the case of 1-butyne, the relaxation rate of the acetylenic hydrogen could be enhanced due to the proximity to a "center of flexibility."<sup>10</sup>

An interesting question is whether or not IVR of the methyl group in methylsilane is comparable to that of the methyl groups in other molecules. Consulting Table IX, it looks like many methyl groups do behave similarly. This generalization should be considered tentative, as the spectra for most of the molecules in Table IX were not eigenstate resolved. A physical basis for a universal behavior of methyl groups could be the presence of a Fermi resonance doorway state, formed by an overtone of the methyl deformation. If a doorway state involves proximate atoms, and the doorway state couples strongly to a generic bath, then the chromophore could be expected to exhibit similar dynamics in a variety of molecules. This could be the case for the methyl group in certain series of molecules.

The results of the present study bear implications in three different directions. First, as shown in other studies, low overtone vibrational energy can remain localized for long times, i.e., on a nanosecond time scale, which implies the possibility for laser induced chemical effects. Second, also as shown in other experiments, IVR is seen to be mode specific, again opening the way to mode specific chemistry. Third, the behavior of the (3,0,0) band could be representative of that of high vibrational levels of a variety of hydrogen oscillators. Since many hydride stretches have been shown to exhibit local mode behavior at high  $\nu$  the investigation of their IVR properties is warranted.

## ACKNOWLEDGMENTS

This work was carried out with the support of the NSF under the Grant No. CHEM-9318725. The support of B.M. by a fellowship from the German academic exchange program (DAAD) is gratefully acknowledged.

## APPENDIX A

This table for (3,0,0) lists most of the observed lines and their integrated intensities along with assignments.

Assignment	Wave number (cm <sup>-1</sup> )	Integrated intensity	
<sup>t</sup> R <sub>1</sub> (3)	6305.072 49	18.01	
	6305.071 73	10.931	
	6305.071 57	6.415	
	6305.070 83	3.885	
	6305.070 79	0.055	
	<sup>t</sup> R <sub>1</sub> (2)	6304.3657	10.35
		6304.3621	5.878
		6304.3585	6.07
		6304.356 39	3.956
		6304.354 33	3.517
6304.348 78		4.501	
6304.343 88		3.468	
6304.343 72		0.132	
6304.3437		6.818	
6304.342 47		12.365	
?	6304.341 73	17.941	
	6304.338 53	23.398	
?	6304.336 76	21.129	
	6304.3357	23.891	
?	6304.334 21	9.647	
	6304.333 86	4.765	
?	6304.333 35	18.791	
	6304.325 45	16.13	
?	6303.637 72	16.436	
	6303.627 43	27.88	
<sup>t</sup> R <sub>1</sub> (1)	6303.625 52	50.509	
	6303.624 82	41.367	
	6303.6209	20.306	
	6303.620 25	47.198	
	6303.6182	41.433	
	6303.617 41	13.641	
	6303.616 41	14.139	
	6303.614 75	207.889	
	6303.614 34	52.345	
	6303.612 13	31.518	
	6303.608 72	34.091	
	6303.605 71	41.009	
	6303.585 19	19.425	
	6303.5833	19.353	
	6303.573 14	19.463	
<sup>t</sup> Q <sub>1</sub>	6302.1629	3.206	
	6302.161 08	14.145	
	6302.160 35	13.807	
	6302.156 49	6.242	
	6302.155 77	18.511	
	6302.1537	11.38	
	6302.153 12	9.642	
	6302.151 84	0.0002	
	6302.150 24	69.06	
	6302.149 83	21.692	
	?	6302.148 31	12.05
		6302.147 62	20.777
		6302.144 33	17.024
	?	6302.142 61	28.071
		6302.141 65	18.209
?	6302.141 28	1.919	
	6302.135 62	21.765	
	6302.118 81	49.198	
<sup>t</sup> R <sub>0</sub> (3)	6302.115 38	3.246	
	6302.064 69	7.806	
<sup>q</sup> R <sub>0</sub> (5)	6302.062 01	54.562	
	6301.404 12	16.192	
<sup>t</sup> R <sub>0</sub> (2)	6301.403 38	8.303	

## APPENDIX A (Continued.)

Assignment	Wave number (cm <sup>-1</sup> )	Integrated intensity
	6301.397 29	233.331
	6301.391 92	48.235
	6301.386 18	21.767
	6301.382 54	10.794
	6301.382 34	13.471
	6301.379 59	20.147
<sup>q</sup> R <sub>0</sub> (4)	6301.338 73	33.565
	6301.336 83	20.748
	6301.333 17	16.182
	6301.332 39	40.529
<sup>q</sup> R <sub>1</sub> (4)	6301.303 29	42.653
	6301.292 73	16.915
	6301.291 9	21.947
	6301.290 71	21.327
	6301.287 06	16.682
?	6300.678 95	74.553
?	6300.672 97	115.61
?	6300.670 89	26.133
?	6300.670 31	100.104
<sup>r</sup> R <sub>0</sub> (1)	6300.663 53	23.505
	6300.663 14	38.171
	6300.661 11	49.881
	6300.658 71	71.669
	6300.656 18	17.881
	6300.655 98	0.172
	6300.655 16	19.576
<sup>q</sup> R <sub>0</sub> (3)	6300.610 32	143.693
	6300.607 75	20.96
<sup>q</sup> R <sub>1</sub> (3)	6300.577 52	24.509
	6300.575 39	12.745
	6300.575 35	0.267
	6300.572 64	29.723
	6300.571 99	26.383
	6300.571 18	14.574
	6300.570 65	11.574
	6300.570 01	37.811
	6300.567 56	24.509
	6300.566 59	39.318
	6300.559 12	22.467
<sup>r</sup> R <sub>0</sub> (0)	6299.947 49	39.337
	6299.946 5	26.739
	6299.936 61	127.605
	6299.936 36	32.365
	6299.934 81	43.753
	6299.928 09	34.685
<sup>q</sup> R <sub>0</sub> (2)	6299.883 67	34.248
	6299.882 32	108.713
<sup>q</sup> R <sub>1</sub> (2)	6299.845 51	38.749
	6299.842 2	80.994
	6299.840 74	31.338
	6299.833 47	31.62
<sup>r</sup> Q <sub>0</sub>	6299.218 06	7.859
	6299.217 67	9.409
	6299.216 33	79.563
	6299.213 51	10.752
	6299.212 9	47.206
	6299.206 67	16.156
	6299.206 43	32.116
	6299.204 75	20.683
	6299.202 6	22.481
	6299.201 5	18.432
	6299.201 18	88.595
	6299.200 6	19.856
	6299.195 89	6.373

## APPENDIX A (Continued.)

Assignment	Wave number (cm <sup>-1</sup> )	Integrated intensity
<sup>q</sup> R <sub>0</sub> (1)	6299.157 93	18.778
	86.934	
	6299.152 92	83.305
	6299.152 31	105.247
<sup>q</sup> R <sub>1</sub> (1)	6299.121 52	54.819
	6299.1183	64.832
	6299.117 95	45.018
	6299.116 44	122.682
	6299.115 79	89.928
	6299.113 47	52.392
	6299.1103	27.532
?	6298.435 63	7.368
?	6298.429 14	9.332
<sup>q</sup> R <sub>0</sub> (0)	6298.424 78	25.958
	6298.423 28	144.159
	6298.419 4	15.691
	6298.417 11	8.843
	6298.416 89	38.542
?	6298.412 37	17.119
?	6298.393 91	10.821
?	6297.736 53	16.915
?	6297.679 88	29.581
?	6297.675 17	3.762
?	6297.675 04	16.643
?	6297.673 82	8.851
?	6297.669 45	10.662
?	6297.6681	10.081
?	6297.662 22	6.983
?	6297.661 97	27.123
?	6297.661 59	12.658
?	6297.660 64	7.22
?	6297.660 36	5.3
<sup>q</sup> Q <sub>1</sub>	6297.6544	17.111
	6297.653 03	12.272
	6297.651 34	144.399
	6297.650 97	0.983
	6297.650 24	169.362
	6297.649 75	65.105
	6297.648 66	32.973
	6297.647 91	25.124
	6297.647 24	22.783
	6297.646 93	10.885
	6297.644 95	19.756
	6297.644 61	15.975
	6297.641 76	21.019
<sup>q</sup> P <sub>0</sub> (1)	6296.957 77	99.262
	6296.9562	59.272
<sup>q</sup> P <sub>0</sub> (2)	6296.226 72	16.279
<sup>q</sup> P <sub>0</sub> (2)	6296.225 17	48.156
<sup>p</sup> Q <sub>1</sub> ?	6296.222 96	52.728
<sup>q</sup> P <sub>0</sub> (2)	6296.221 24	4.883
<sup>q</sup> P <sub>0</sub> (2)	6296.2188	21.488
<sup>p</sup> Q <sub>1</sub> ?	6296.218 49	6.468
?	6296.217 56	27.943
<sup>p</sup> Q <sub>1</sub> ?	6296.216 41	23.322
<sup>p</sup> Q <sub>1</sub> ?	6296.214 36	16.929
<sup>p</sup> Q <sub>1</sub>	6296.2085	29.328
<sup>p</sup> Q <sub>1</sub> ?	6296.207 91	22.694
<sup>p</sup> Q <sub>1</sub> ?	6296.205 76	14.664
<sup>p</sup> Q <sub>1</sub>	6296.204 45	74.291
<sup>p</sup> Q <sub>1</sub> ?	6296.199 66	19.195
<sup>p</sup> Q <sub>1</sub> ?	6296.198 19	33.473
<sup>p</sup> Q <sub>1</sub>	6296.197 72	46.409
<sup>q</sup> P <sub>2</sub> (2)	6296.192 11	1.26

## APPENDIX A (Continued.)

Assignment	Wave number (cm <sup>-1</sup> )	Integrated intensity
	6296.190 73	4.836
	6296.189 16	44.927
	6296.188 86	0.08
	6296.188 06	46.824
	6296.187 55	23.504
	6296.186 41	14.452
	6296.185 65	5.625
	6296.185 03	3.183
	6296.184 67	2.534
	6296.183 25	10.96
	6296.182 49	6.38
	6296.179 49	9.384
<sup>q</sup> P <sub>0</sub> (3)	6295.492 16	5.803
	6295.489 33	18.898
	6295.487 26	18.112
	6295.486 63	23.487
?	6295.485 72	72.505
?	6295.482 14	8.511
<sup>p</sup> P <sub>1</sub> (1)	6295.474 03	39.12
	6295.467 11	22.454
	6295.466 72	6.241
	6295.462 9	28.826
	6295.461 89	19.402
<sup>q</sup> P <sub>1</sub> (3)	6295.455 75	11.789
	6295.452 53	16.325
	6295.452 14	2.98
	6295.450 66	26.909
	6295.449 99	23.401
	6295.447 7	13.636
	6295.444 55	3.924
?	6294.755 88	22.112
<sup>q</sup> P <sub>0</sub> <sup>p</sup> (4)	6294.754 18	3.319
<sup>q</sup> P <sub>0</sub> <sup>p</sup> (4)	6294.752 8	29.851
?	6294.749 38	7.337
<sup>p</sup> P <sub>1</sub> (2)	6294.741 45	13.203
	6294.737 44	25.603
	6294.730 73	17.511
<sup>q</sup> P <sub>1</sub> (4)	6294.716	8.525
	6294.712 73	19.437
	6294.711 47	4.565
	6294.704 18	3.068

## APPENDIX B

This table for  $2\nu_7^0$  lists most of the observed lines and their integrated intensities along with assignments.

Assignment	Wave number (cm <sup>-1</sup> )	Integrated intensity
<i>R</i> (5) region	5912.629 62	
	5912.627 18	28.242
	5912.623 4	5.024
	5912.621 83	5.48
	5912.621 06	9.617
	5912.616 12	32.779
	5912.615 63	20.313
	5912.613 22	21.462
	5912.609 21	7.605
	5912.599 48	12.356
	5912.578 76	32.605
<i>R</i> (4)	5911.920 84	11.331
<i>R</i> (4)	5911.913 51	27.745
?	5911.907 5	11.983

## APPENDIX B (Continued.)

Assignment	Wave number (cm <sup>-1</sup> )	Integrated intensity
<i>R</i> (4)	5911.905 65	18.559
?	5911.902 23	17.216
<i>R</i> (4)	5911.901 88	19.367
<i>R</i> (4)	5911.901 29	24.895
?	5911.895 72	9.522
?	5911.894 27	10.675
<i>R</i> (4)	5911.893 53	21.585
<i>R</i> (4)	5911.891 75	38.477
<i>R</i> (4)	5911.889 84	93.03
?	5911.883 67	15.872
?	5911.880 4	22.308
?	5911.875 11	12.871
?	5911.861 99	15.235
?	5911.855 11	14.492
?	5911.852 31	28.035
?	5911.848 61	18.727
?	5911.255 2	19.631
?	5911.239 24	6.179
?	5911.237 64	6.554
?	5911.236 43	19.036
?	5911.233 8	23.076
?	5911.231 79	6.92
<i>R</i> (3)	5911.206 82	10.804
?	5911.205 11	10.009
?	5911.197 99	10.137
?	5911.195 49	5.332
?	5911.194 58	15.381
<i>R</i> (3)	5911.19	17.103
<i>R</i> (3)	5911.188 17	51.725
<i>R</i> (3)	5911.187 58	27.97
<i>R</i> (3)	5911.185 46	2.144
<i>R</i> (3)	5911.184 88	45.448
?	5911.181 18	18.699
<i>R</i> (3)	5911.174 52	9.225
?	5911.173 12	14.515
?	5911.169 86	4.807
?	5911.168 9	10.389
<i>R</i> (3)	5911.166 96	17.305
<i>R</i> (3)	5911.165 1	79.462
<i>R</i> (3)	5911.162 64	7.534
?	5911.160 85	3.805
?	5911.158 47	10.322
?	5911.152 37	16.199
?	5911.148 73	12.387
<i>R</i> (3)	5911.142 55	27.422
?	5911.141 15	11.489
?	5911.140 11	8.301
?	5911.137 21	15.053
?	5911.121 22	10.358
?	5910.576 67	41.257
	5910.569 48	59.148
?	5910.483 74	26.929
	5910.481 44	7.105
	5910.471 24	9.933
<i>R</i> (2)	5910.468 64	200.604
	5910.467 34	41.105
	5910.463 56	30.11
	5910.459 42	47.548
	5910.458 33	18.903
	5910.455 76	61.985
	5910.454 37	43.367
	5910.453 55	7.995
	5910.450 89	8.219

## APPENDIX B (Continued.)

Assignment	Wave number ( $\text{cm}^{-1}$ )	Integrated intensity
	5910.448 74	26.853
	5910.447 95	15.534
	5910.445 8	9.682
	5910.441 83	11.263
	5910.440 12	16.056
	5910.435 61	35.791
	5910.432 73	46.613
	5910.431 7	9.477
	5910.431 23	34.247
	5910.422 28	23.228
	5910.417 23	55.511
	5910.408 26	16.725
	5910.407 11	11.479
	5910.396 67	15.036
?	5910.387 85	7.443
	5910.384 64	10.69
	5910.378 74	10.439
	5910.357 24	10.404
	5910.353 84	6.377
	5910.349 14	8.848
	5910.340 25	11.273
	5910.334 45	20.79
	5910.317 79	11.73
?	5909.892 79	24.096
	5909.883 72	31.239
	5909.876 72	14.952
	5909.875 4	24.269
	5909.871 72	21.997
	5909.865 88	5.308
	5909.853 92	21.327
	5909.810 76	18.6
	5909.801 82	22.464
	5909.786 73	14.027
	5909.780 96	12.49
	5909.780 7	7.895
	5909.778 6	19.978
	5909.774 97	19.861
	5909.771 51	12.441
R(1)	5909.767 31	10.12
	5909.767 02	36.092
	5909.766 21	36.166
	5909.763 61	30.093
	5909.761 05	21.856
	5909.760 07	55.051
	5909.759 6	42.755
	5909.748 66	24.06
	5909.747 69	90.13
	5909.742 67	283.033
	5909.739 83	15.952
	5909.737 91	17.396
	5909.736 67	16.698
	5909.734 55	19.572
	5909.731 43	20.478
	5909.731 23	45.7
	5909.727 5	31.638
	5909.725 22	13.644
	5909.721 34	19.194
	5909.719 96	13.0696
	5909.716 64	39.979
	5909.715 09	78.259
	5909.710 02	50.213
	5909.709 67	54.038
	5909.702 53	29.839
	5909.695 71	12.082

## APPENDIX B (Continued.)

Assignment	Wave number ( $\text{cm}^{-1}$ )	Integrated intensity
	5909.694 69	17.319
	5909.688 77	43.629
	5909.687 21	21.788
	5909.683 79	34.873
	5909.681 52	38.567
	5909.661 76	10.455
	5909.658 61	31.226
	5909.645 02	7.041
	5909.644 34	32.441
?	5909.630 75	12.102
?	5909.621 01	27.245
?	5909.602 26	17.281
?	5909.571 65	12.349
?	5909.556 5	8.575
?	5909.539 9	18.79
R(0)	5909.031 55	267.161
?	5909.027 68	166.001
R(0)	5909.006 23	639.276
R(0)	5908.995 42	342.37
?	5908.974 21	44.415
?	5908.963 79	37.42
R(0)	5908.950 15	210.436
R(0)	5908.915 68	55.537
R(0)	5908.915 19	66.536
?	5908.427 45	87.298
Q	5908.415 91	280.456
?	5908.385 14	70.543
Q	5908.370 63	55.615
Q	5908.359 24	57.87
?	5908.323 52	75.478
Q	5908.314 21	86.819
Q	5908.312 51	33.519
Q	5908.299 65	105.804
Q	5908.295 14	268.2
?	5908.286 91	68.285
?	5908.281 16	32.031
Q?	5908.276 05	58.879
Q	5908.270 04	326.22
?	5908.260 74	29.696
?	5908.250 06	17.258
?	5908.246 39	49.118
Q	5908.245 52	342.108
Q	5908.242 74	35.054
Q	5908.241 04	142.289
Q	5908.239 31	59.226
Q	5908.230 84	111.724
Q	5908.219 64	152.225
Q	5908.206 34	335.124
Q	5908.197 64	45.271
Q	5908.195 24	80.009
Q	5908.191 24	61.293
Q	5908.188 65	31.921
Q	5908.185 15	43.535
Q	5908.183 18	17.287
?	5907.935 92	11.463
	5907.847 38	9.083
P(1) region	5907.579 8	
	5907.557 29	174.05
	5907.551 5	10.85
	5907.540 96	65.81
	5907.533 69	32.055
	5907.521 77	18.884
	5907.490 68	73.344
	5907.475 08	12.092

## APPENDIX B (Continued.)

Assignment	Wave number ( $\text{cm}^{-1}$ )	Integrated intensity
?	5906.9631	10.918
$P_1(2)$	5906.951 59	127.432
$P_1(2)$	5906.906 29	33.246
$P_1(2)$	5906.894 99	7.877
$P_1(2)$	5906.85	65.306
$P_1(2)$	5906.848 33	34.725
$P_0(2)$	5906.8375	221.385
$P_1(2)$	5906.8355	23.918
?	5906.833 46	71.607
$P_1(2)$	5906.830 96	83.699
$P_0(2)$	5906.812 04	318.837
$P_1(2)$	5906.805 82	112.002
$P_0(2)$	5906.801 22	152.602
$P_1(2)$	5906.781 38	147.353
$P_1(2)$	5906.778 41	47.859
$P_1(2)$	5906.776 94	38.906
$P_1(2)$	5906.775 28	24.258
$P_1(2)$	5906.766 69	66.837
$P_0(2)$	5906.755 92	54.204
$P_1(2)$	5906.755 69	80.329
$P_1(2)$	5906.742 36	151.259
$P_1(2)$	5906.733 61	22.899
$P_1(2)$	5906.731 15	10.974
$P_1(2)$	5906.727 11	36.073
$P_1(2)$	5906.724 71	20.903
$P_0(2)$	5906.721 19	116.792
$P_0(2), P_1(2)$	5906.721 09	
$P_1(2)$	5906.719 09	16.755
?	5906.618 94	53.969
$P(3)$	5906.093 67	11.877
	5906.093 35	15.981
	5906.092 53	32.171
	5906.089 88	11.9
	5906.087 36	25.316
	5906.086 35	26.405
	5906.085 94	66.204
	5906.074 86	81.608
	5906.073 93	76.569
	5906.068 91	206.207
	5906.066 03	11.608
	5906.0642	13.605
	5906.062 85	34.566
	5906.060 81	16.454
	5906.057 61	40.996
	5906.057 21	20.291
	5906.053 75	21.356
	5906.051 79	6.628
	5906.047 44	11.068
	5906.045 77	6.971
	5906.042 87	13.726
	5906.041 29	54.752
	5906.036 19	41.11
	5906.035 58	4.723
	5906.028 69	13.502
	5906.0218	11.005
	5906.020 84	9.416
	5906.014 99	22.558
	5906.013 24	36.638
	5906.009 92	35.628
	5906.007 72	28.381
	5905.987 93	7.837
	5905.984 75	10.381
	5905.971 09	30.814
	5905.970 51	40.967

## APPENDIX B (Continued.)

Assignment	Wave number ( $\text{cm}^{-1}$ )	Integrated intensity
$P(4)$	5905.344 21	131.396
	5905.342 86	19.779
	5905.3391	13.317
	5905.335 09	14.955
	5905.333 63	16.04
	5905.331 18	31.364
	5905.329 91	39.875
	5905.329 09	4.442
	5905.326 36	4.26
	5905.324 45	25.941
	5905.323 43	10.226
	5905.321 14	16.155
	5905.317 19	22.325
	5905.315 48	18.592
	5905.311 08	18.954
	5905.308 32	23.642
	5905.307 28	9.342
	5905.306 72	16.262
	5905.297 83	12.036
	5905.292 75	37.121
	5905.283 95	31.841
	5905.282 55	6.381
	5905.272 07	45.916
$P(5)$	5904.623 58	17.404
	5904.6067	3.906
	5904.604 88	21.009
	5904.604 29	5.687
	5904.601 97	11.783
	5904.601 47	11.307
	5904.591 32	5.996
	5904.583 81	14.542
	5904.581 83	33.223
	5904.579 51	13.011
	5904.559 42	30.452

<sup>1</sup>D. Wardlaw and R. Marcus, *Adv. Chem. Phys.* **70**, 231 (1987).<sup>2</sup>K. Lehmann, G. Scoles, and B. Pate, *Annu. Rev. Phys. Chem.* **45**, 241 (1994).<sup>3</sup>D. Nesbitt and R. Field, *J. Phys. Chem.* **100**, 12735 (1996).<sup>4</sup>E. Heller, *Faraday Discuss. Chem. Soc.* **75**, 141 (1983).<sup>5</sup>J. Gambogi *et al.* *Chem. Phys.* **190**, 191 (1995).<sup>6</sup>J. Timmermans, Ph.D. thesis, Princeton University, Princeton, New Jersey, 1994.<sup>7</sup>J. Gambogi, J. Timmermans, K. Lehmann, and G. Scoles, *J. Chem. Phys.* **99**, 9314 (1993).<sup>8</sup>J. Go, T. Cronin, and D. Perry, *J. Chem. Phys.* **175**, 127 (1993).<sup>9</sup>A. McIlroy and D. J. Nesbitt, *J. Chem. Phys.* **92**, 2229 (1990).<sup>10</sup>G. Bethardy and D. Perry, *J. Chem. Phys.* **98**, 6651 (1993).<sup>11</sup>K. Lehmann and G. Scoles (unpublished).<sup>12</sup>P. Brumer and M. Shapiro, *Adv. Chem. Phys.* **70**, 365 (1988).<sup>13</sup>Y. Choi and C. Moore, *J. Chem. Phys.* **94**, 5414 (1991).<sup>14</sup>G. Scherer, K. Lehmann, and W. Klemperer, *J. Chem. Phys.* **78**, 2817 (1983).<sup>15</sup>A. McIlroy *et al.* *J. Chem. Phys.* **100**, 2596 (1994).<sup>16</sup>A. McIlroy, Ph.D. thesis, University of Colorado, Boulder, Colorado, 1991.<sup>17</sup>M. Quack, *Annu. Rev. Phys. Chem.* **41**, 839 (1990).<sup>18</sup>M. Quack, *J. Phys. Chem.* **97**, 12574 (1993).<sup>19</sup>Q. Zhu, B. Zhang, Y. Ma, and H. Qian, *Spectrochim Acta A* **46**, 1217 (1990).<sup>20</sup>D. McKean, A. Morrison, and M. Kelly, *Chem. Phys. Lett.* **109**, 347 (1984).<sup>21</sup>J. Duncan, A. Ferguson, and D. McKean, *J. Mol. Spectrosc.* **168**, 522 (1994).

- <sup>22</sup>M. Child and L. Halonen, *Adv. Chem. Phys.* **57**, 1 (1984).
- <sup>23</sup>E. Kerstel *et al.* *J. Phys. Chem.* **95**, 8282 (1991).
- <sup>24</sup>The methylsilane was purchased from United Technologies, Bristol, Pennsylvania, and used as supplied. The purity was stated to be at least 97%.
- <sup>25</sup>The buildup cavity is a modified core of a Newport model SR-170-C SuperCavity optical spectrum analyzer.
- <sup>26</sup>N. Moazzen-Ahmadi and I. Ozier, *J. Mol. Spectrosc.* **123**, 26 (1987).
- <sup>27</sup>E. Kerstel, K. Lehmann, B. Pate, and G. Scoles, *J. Chem. Phys.* **100**, 2588 (1994).
- <sup>28</sup>B. Pate, K. Lehmann, and G. Scoles, *J. Chem. Phys.* **95**, 3891 (1991).
- <sup>29</sup>W. Lawrence and A. Knight, *J. Chem. Phys.* **89**, 917 (1985).
- <sup>30</sup>K. Lehmann, *J. Chem. Phys.* **95**, 7556 (1991).
- <sup>31</sup>D. Romanini and K. Lehmann, *J. Chem. Phys.* **98**, 6437 (1993).
- <sup>32</sup>E. Hirota, *J. Mol. Spectrosc.* **43**, 36 (1972).
- <sup>33</sup>H. Jagannath, I. Ozier, and N. Moazzen-Ahmadi, *J. Mol. Spectrosc.* **119**, 313 (1986).
- <sup>34</sup>A. McIlroy and D. J. Nesbitt, *J. Chem. Phys.* **101**, 3421 (1994).
- <sup>35</sup>J. Timmermans, K. Lehmann, and G. Scoles, *Chem. Phys.* **190**, 393 (1995).
- <sup>36</sup>K. Lehmann, *J. Chem. Phys.* **95**, 2361 (1991).
- <sup>37</sup>H. Dai, C. Korpa, J. Kinsey, and R. Field, *J. Chem. Phys.* **82**, 1688 (1985).
- <sup>38</sup>J. Go, G. Bethardy, and D. Perry, *J. Phys. Chem.* **94**, 6153 (1990).